Original Article

Grain size and sintering temperatures effects on the mechanical properties of ZnO nanoparticle-based varistor ceramics

Rabab Sendi[1]

Received: 11 August 2022 / Accepted: 9 September 2022
Published online: 28 October 2022

Abstract
The grain size impact on the behavior of ZnO–Bi_2O_3–Mn_2O_3 varistors was determined in this study. Samples with different sintering temperatures and times were prepared via traditional ceramic methodology, and their properties were described. Results exhibited that various temperatures and times of the sintering process had considerable effects on the varistors. In particular, the growth of ZnO grains was improved at a minimal-temperature sintering process of 900 °C for 1 h. Significant solid-state reaction even at lower sintering temperatures perhaps caused the surface characteristics of ZnO nanoparticles. Vickers indentation analyses were applied to define the fracture toughness and hardness of the samples. Hardness diminished with the growth of ZnO grain. Fracture toughness did not exhibit any change with the increase in grain size (~ 5.1 $MPam^{0.5}$) up to 1.6 µm for WZ-V and 3.5 µm 20Z-V. Above these grain sizes, a spontaneous conversion from hexagonal to monoclinic phase occurred. WZ-V and 20Z-V samples were used to investigate the analogous bending strength at 1152 and 1148 MPa, respectively. The structural coarsening desired for realizing significant grain size led to increased scattering strength values, as evidenced by lesser Weibull modulus (9.23 vs. 5.10). Variations in the mechanical behavior of the investigated varistors with different grain sizes were demonstrated, and their probable reasons were discussed in brief.

Keywords Mechanical properties · ZnO · Nanoparticles · Sintering · Microstructure

1 Introduction

Varistor discs have been utilized in electrical and electronic equipment, such as surge protection system, for various decades attributed to their exceptional nonlinearity behavior and minimal leakage current. The breakdown voltage and resistance values of these samples massively relies on the structural situations; therefore, grain size and homogeneity of structure are the highest considerable parameters within the fabrication process of varistor samples [1]. One technique to accomplish these aims is to apply homogeneous 20-nm ZnO for sample production. The homogeneity of ZnO nanoparticles is a requisite for superior fabrication of varistor samples. Thus, the development of the homogenous microstructure of varistors is a requisite for the enhancement of the electronic, electrical, and mechanical behaviors of disc samples [2].

ZnO nano crystallites possess varied chemical and physical behavior in comparison with raw materials. Greater homogeneity, better ability of sintering process, and other remarkable characteristics may be expected due to their nano-scale particles and several surface characteristics [3]. Therefore, the behavior of varistor samples with ZnO nanoparticles must be developed extensively when manufacturing them.

The relationships among the microstructural and mechanical characteristics of varistor discs have been discussed considerably in the past years. The effect of

✉ Rabab Sendi, rksendi@uqu.edu.sa | [1]Department of Physics, Faculty of Applied Science, Umm Al-Qura University, Makkah, Saudi Arabia.

J.Umm Al-Qura Univ. Appll. Sci. (2022) 8:50–56 | https://doi.org/10.1007/s43994-022-00002-9

conversion toughening (stress-produced transformation from hexagonal to monoclinic phase) within the varistor is currently suggested to be generally based on grain size [4, 5]. The greater the hexagonal ZnO grains are, the larger predilection to subject stress-produced conversion to a stability microstructure, leading to promoted toughness. The highest toughness is situated close the crucial grain size, in which the hexagonal ZnO grains are subject to hexagonal-to-monoclinic transformation [4]. Therefore, microstructural parameters, such as grain size distribution, porosity, phase aggregation, and purity, are assumed to be considered in varistor microstructure.

In this work, the effect of different grain sizes of ZnO on the mechanical properties of ceramic discs compared with that of commercial samples manufactured using micro particles ZnO was obtained. A commercial ceramic process technique was utilized to produce varistors by using nanosized powder, and different sintering temperatures and times were applied.

2 Methodologies

2.1 Sample preparation

Two ZnO powders were utilized for the manufacturing of examination samples by the traditional ceramic technique including ball milling, drying, pressing, andn sintering. Oxide powders with 99.9% purity were applied. The structure composed of 99 mol% 20-nm ZnO for ZnO nanoparticles-based varistor (20Z-V) or 99 mol% White ZnO for micro ZnO-based varistor (WZ-V) + 0.5 mol% Bi_2O_3 + 0.5 mol% Mn_2O_3 powder for both varistors. The raw materials applied in this work were of significant purity and quality. Below are the raw materials list and their corresponding properties. The technical specifications of the raw materials are posted in following table.

Material	Chemical formula	Purity (%)	Mean size	Supplier
Nanoparticles zinc oxide	ZnO	> 99.9	20 nm	Mknano, Canada
Zinc oxide (white)	ZnO	> 99.8	0.23 µm	Appro, Malaysia
Bismuth trioxide	Bi_2O_3	> 99.9	10 µm	Segma-Aldaich
Manganese trioxide	Mn_2O_3	> 99.9	0.7 µm	Segma-Aldaich

The powder was blended with poly vinyl alcohol (PVA) by mixing with distilled water in a ball milling jar for 6 h. The ZnO slurry was dried at 60 °C in air for 1 h and then was granulated by sieving through a 20-mesh sieve. The producing granules were utilized to fabricate discs via pressing at 4 ton/cm^2 pressure. The green ZnO discs were 26 mm in diameter and 2 mm thick. Lastly, the green discs were sintered at 900 °C, 1200 °C, and 1400 °C in air for 3 h and time with 2 °C/min heating rate and cooling normally.

2.2 Characterization

The sintered ceramics relative densities aligned with different sintering temperatures were measured applying Archimedes technique in de-ionized water. The microstructure of the varistor was investigated utilized a scanning electron microscopy (SEM) system (model: JSM-6460 LV). The average grain size (d) was calculated via the estimate on the SEM photos by the linear intercept method [6–8] with the term d = 1.56L/MN, where L is the length of random line on the SEM micrograph, M is the micrograph magnification, and N is the grain boundaries numbers intercepted by lines.

2.3 Mechanical testing

Vickers indentation testing (LV 400, Leco, USA) was applied for the valuation of hardness and fracture toughness. Hardness analysis was conducted at 9.8 N (1 kg) load and 15 s hold. The following equation was employed to determine Vickers hardness, HV (MPa):

$$\mathrm{HV} = 1.8544\, P/d^2 \tag{1}$$

where P is the used load, and d is the mean diagonal line length of the indentation. Ten indentations were formed for every disc. Toughness was estimated immediately from the lengths of cracks created via Vickers indentation through upper loads. The used loads were 98 (10 kg), 196 (20 kg), 294 (30 kg), and 392 (40 kg) N, with a 15 s hold. Crack length was calculated directly after indentation by using a standardized optical microscope. Fracture toughness, K_{Ic}, was measured utilizing the expression presented by Niihara et al. [9] for Palmqvist cracks:

$$K_{\mathrm{Ic}} = 9.052 \times 10^{-3} H^{3/5} E^{2/5} dc^{-1/2}, \tag{2}$$

where H is the hardness, E is the Young's modulus, d is the length of mean diagonal line of the indentation, and c is the Palmqvist crack length. Ten valid measurements were investigated for every varistor. The valid measurements had to satisfy the conditions of JIS R 1607 on satisfactory indentation cracks.

Flexural strength was obtained for the chosen varistor discs in four-point bending at a crosshead speed of 2 mm/min, applying completely expressive fixture with a 10 mm inner and 20 mm outer span. Ceramic bars with

dimensions ca. $2.5 \times 2 \times 25$ mm^3 were cut from the samples, ground, and polished. Weibull strength distribution parameters were computed qualitatively.

3 Results and discussion

3.1 Microstructural analysis

3.1.1 Scanning electron microscopy

Diverse sintering procedures were used in the varistor green discs to achieve intensive sintered samples with various grain sizes of ZnO. The microstructure overview of the ZnO–Bi_2O_3–Mn_2O_3 varistors manufactured from micro- and nano-ZnO particles at several sintering conditions is presented in Fig. 1. The predominant constituent was relatively ZnO grains. Bi-rich phases were furthermore existent within considerable ZnO grains boundaries among grains and at ZnO cluster grain agglomerations.

Most of the aspects of the varistor sample structure are conventional with the ZnO nanoparticle sample, which was subjected to liquid-phase sintering process. The ZnO–Bi_2O_3–Mn_2O_3 varistor samples were principally sintered at very elevated temperature (900–1400 °C) that was beyond the Bi_2O_3 melting point. Thus, the samples were solidified via sintering liquid phase, and amorphous and crystalline phases, which acted as a cement to binder the varistor grains conjointly, were formed through the cooling step of this phases.

The SEM images in Fig. 1 exhibited that the morphology of the varistor surface was substantially based on the sintering process conditions and the mean ZnO grains size and grains density development during the optimal density at 1200 °C for 2 h.

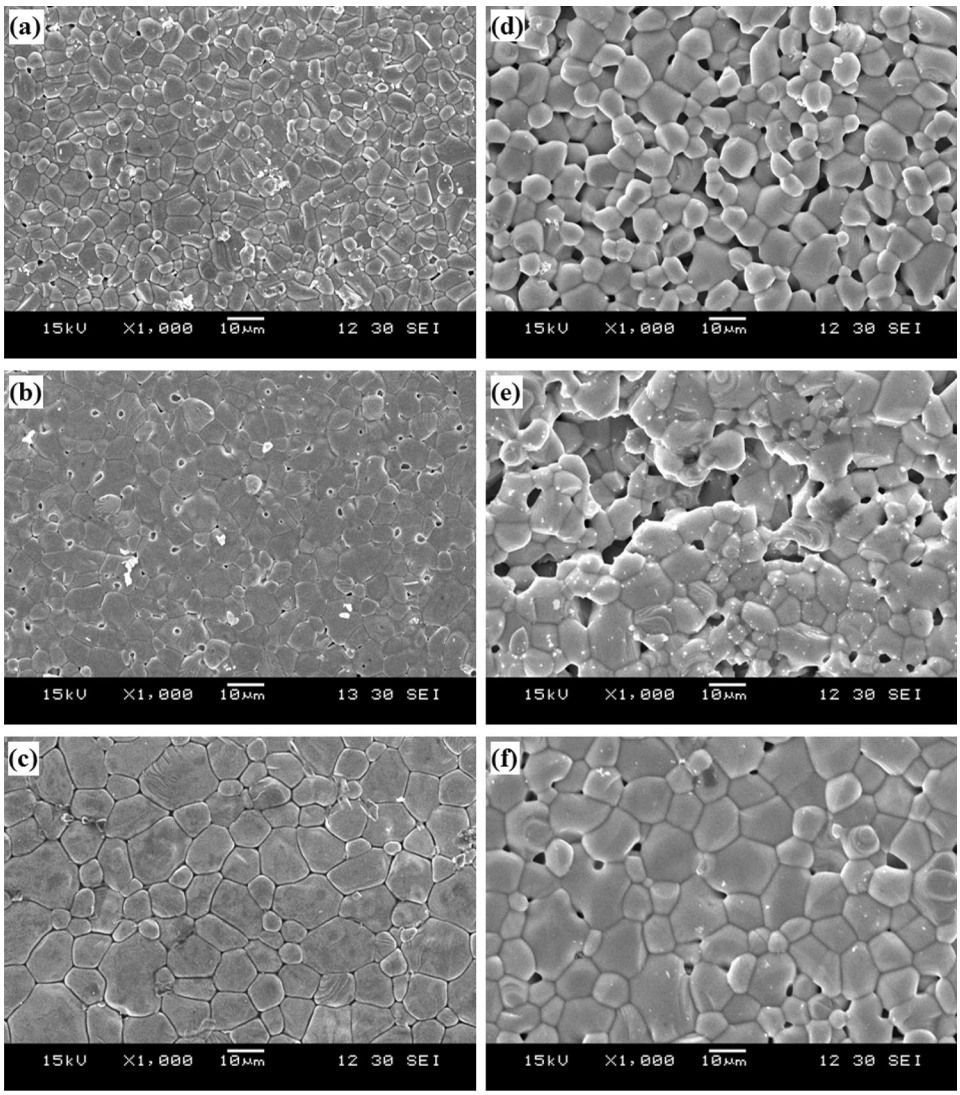

Fig. 1 Typical SEM images of WZ-V ceramics sintered at **a** 900 °C, **b** 1200 °C, and **c** 1400 °C for 3 h; and 20Z-V ceramics sintered at **d** 900 °C, **e** 1200 °C, and **f** 1400 °C for 3 h

The ZnO particles had small-grains sized structures with the morphology changing according to the variation in the sintering temperatures. The SEM images show that the grain boundaries were fewer and the grains grew much bigger with further increase of sintering temperature. The high sintering temperature provides more activation energy to atoms to grow larger grains. Lin et al. [10] described that high temperature can stimulate the migration of grain boundaries and cause the coalescence of more grains during the annealing processes. Fang et al. [11] further indicated at high temperature, more energy should be available for the atoms to acquire so that they may diffuse and occupy the correct site in the crystal lattice and grains with lower surface energy will grow larger at high temperature.

Furthermore, the average sample density was reduced as the sintering time and the temperature was increased to 1400 °C. The varistor structure continued to be very cohesive and dense, but the disc's theoretical density was reduced, which could be attributed to the instantaneous transformation of hexagonal phase to monoclinic phase (Table 1).

The ZnO grains turned into further structured and looked like hexagons or polygons. Their porosity was minimal, but they grew larger. An elevated temperature of the sintering process for a long time is well recognized to give a huge driving force for interior atomic dispersion, which is important for the ZnO grains growth and the porosity elimination. The elevated varistor densification at high temperatures during the sintering process was possibly due to the Bi_2O_3 and Mn_2O_3 doping impacts within the lattice of ZnO crystal, which led to the oxygen vacancies creation through the sintering step. As the dopant ions were recompensed in the Zn ion site through the sintering step, oxygen vacancies were formed, participating to the improvement of the ZnO varistor disc density.

Table 1 Microstructural and physical parameters of WZ-V and 20Z-V ceramics sintered at different temperature and time

Sample	Sintering schedule (°C)/(h)	Grain size d (μm)	Sintering density ρ (g/cm^3)	Relative density ρ_{re} (% t.d.)
WZ-V	900/1	0.3	5.244	93.0
WZ-V	900/2	0.5	5.259	93.6
WZ-V	900/3	0.9	5.290	94.5
WZ-V	1200/1	1.4	5.389	96.4
WZ-V	1200/2	1.9	5.440	97.0
WZ-V	1200/3	2.7	5.412	96.0
WZ-V	1400/1	3.2	5.216	92.2
WZ-V	1400/2	3.5	5.209	91.8
WZ-V	1400/3	3.9	5.200	91.6
20Z-V	900/1	1.8	5.389	94.9
20Z-V	900/2	2.2	5.440	95.3
20Z-V	900/3	2.8	5.490	96.3
20Z-V	1200/1	3.5	5.440	95.5
20Z-V	1200/2	3.8	5.420	95.4
20Z-V	1200/3	4.3	5.380	94.6
20Z-V	1400/1	5.1	5.300	93.6
20Z-V	1400/2	5.6	5.250	92.8
20Z-V	1400/3	6.3	5.209	91.9

A temperature of 900 °C for 1 h was the minimal temperature applied in the sintering process for the varistors; it was needed to achieve a dense sintered disc. Huge grains were investigated at longer times and higher temperatures through the sintering step. The sintering program schedules and the densities formation and ZnO grain sizes are exhibited in Table 1. The average grain size of the WZ-V samples varied between 0.3 (sintered at 900 °C/1 h) and 3.6 μm (sintered at 1400 °C/3 h). The crucial size of ZnO grain for instantaneous conversion from hexagonal to monoclinic phase ranged from 1.8 to 2.15 μm, where the monoclinic phase existing within the WZ-V ceramics developed significantly. The varistor disc sintered during 1400 °C for 3 h contained 55% monoclinic phase, and it was roughly cracked because of volume-alteration-associated t → m conversion. Many researchers [10–12] have obtained significant cubic grains during heat treatment of WZ-V discs. In the present work, no considerable development of grains was noted through the microstructure coarsening.

The 20Z-V samples may be dense at minimal temperature and shorter dwell time compared with the bulk one due to small size of particle and huge ratio of surface-to-volume for 20 ZnO nanoparticle powders. Microstructure coarsening was investigated using high-temperature sintering process. The results showed that the growth kinetics of the grain between the 20Z-V and WZ-V samples was diverse. The 20Z-V samples sintered at 1200 °C for 1 h achieved bigger grains than the WZ-V samples sintered under similar conditions (1.5 vs. 1.4 μm). Furthermore, the density of the 20Z-V samples was obviously reduced at small grain size, in which no existent monoclinic phase was observed. Figure 2 indicates the density of the varistor as a function of ZnO grain size for both samples.

3.2 Mechanical properties

Vickers hardness analysis was conducted in every sample. The mean values of hardness are presented in Table 2. The hardness of the WZ-V samples decreased with increasing grain size, as shown in Fig. 3, which exhibits the WZ-V hardness as a function of the inverted grain size square root. The values of graph could be appropriated with a line ($r^2 = 0.94$), which demonstrated that this reliance applied the relationship of Hall–Petch. The 20Z-V samples hardness

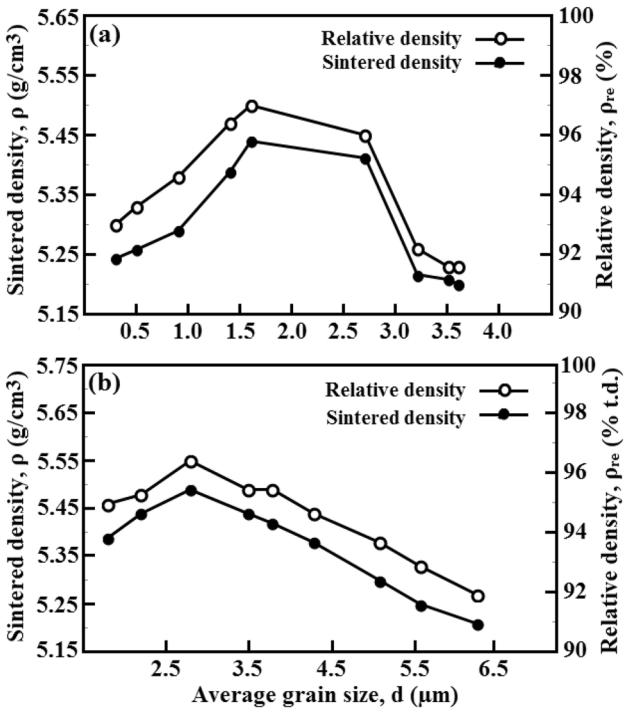

Fig. 2 The sintered and relative densities of **a** WZ-V at 900 °C, 1200 °C and 1400 °C/1, 2, 3 h and **b** 20Z-V ceramics at 900 °C, 1200 °C and 1400 °C/1, 2, 3 h as a function of grain size

indicated a very high dissipation. However, the linear fit appeared to be acceptable. Several fit parameters (lesser hardness of 20Z-V discs than WZ-V discs) may be due to various grain sizes and structures of the phase (mixed hexagonal-cubic vs. pure hexagonal).

Several Vickers indenter loads within the area between 98 (10 kg) and 392 (40 kg) N were applied to create cracks within the varistor discs. For all samples, a Palmqvist cracks only were generated. The values of fracture toughness estimated from the lengths of crack by applying Eq. (2) through various loads are presented by Table 2. The 98 N (10 kg) indenter load formed unstable cracks, which increased after load liberation. Determining the crack length properly was very difficult; thus, the toughness of the fracture investigated via such load is not involved in Table 2. Figure 4a presents that the reliance of fracture toughness of the WZ-V samples at various loads at grain size. The fracture toughness values varied significantly with various loads. Therefore, the reliance of toughness on size of grain presented a similar tendency for different loads. A mean of values specified at various loads is determined in Table 2 to achieve the most dependable fracture toughness values. The graphs in Fig. 5 showed the average fracture toughness dependence on size of grain for the WZ-V and 20Z-V samples. This reliance could be separated into dual regions. The values of toughness were nearly constant with the increase in grain size (~ 5.1 $MPam^{0.5}$) up to 1.6 μm for WZ-V and 3.5 μm for 20Z-V. With the increase in grain size, the toughness increased linearly (8.5 $MPam^{0.5}$) up to 3.6 μm grain size for WZ-V and 6.3 μm for 20Z-V. Beyond this size, conversion to monoclinic phase occurred, as reported by Quinn and Bradt [13]. Figure 5 indicates that the WZ-V and 20Z-V samples subjected the

Table 2 Hardness (HV) and fracture toughness (K_{Ic}) of WZ-V and 20Z-V ceramics sintered at different temperature and time

Sample	Sintering schedule (°C)/(h)	Hardness, HV (MPa)	Fracture toughness, K_{Ic} ($MPam^{0.5}$)				
			10 kg	20 kg	30 kg	40 kg	Average
WZ-V	900/1	13,871	5.04	5.50	5.23	5.87	5.41
WZ-V	900/2	13,298	5.13	5.55	5.32	5.51	5.38
WZ-V	900/3	12,952	5.10	5.60	5.26	5.44	5.35
WZ-V	1200/1	12,732	5.22	5.80	5.38	5.48	5.47
WZ-V	1200/2	11,989	5.80	5.41	5.93	6.13	5.82
WZ-V	1200/3	11,812	6.54	6.00	5.73	6.81	6.27
WZ-V	1400/1	11,522	7.23	6.54	6.80	7.40	6.99
WZ-V	1400/2	10,770	8.12	7.34	7.80	8.10	7.84
WZ-V	1400/3	10,640	8.72	8.12	8.94	7.91	8.42
20Z-V	900/1	16,522	5.24	5.42	5.80	5.92	5.60
20Z-V	900/2	15,746	5.11	5.76	5.88	6.13	5.72
20Z-V	900/3	15,420	5.32	5.44	5.72	6.22	5.68
20Z-V	1200/1	15,198	5.50	5.75	6.00	6.20	5.74
20Z-V	1200/2	14,731	5.76	5.98	6.22	6.51	6.12
20Z-V	1200/3	14,425	6.23	5.87	6.43	6.60	6.28
20Z-V	1400/1	13,529	6.44	6.81	6.92	7.53	6.93
20Z-V	1400/2	13,410	7.34	7.76	7.23	7.67	7.50
20Z-V	1400/3	13,066	8.17	8.45	8.71	8.88	8.55

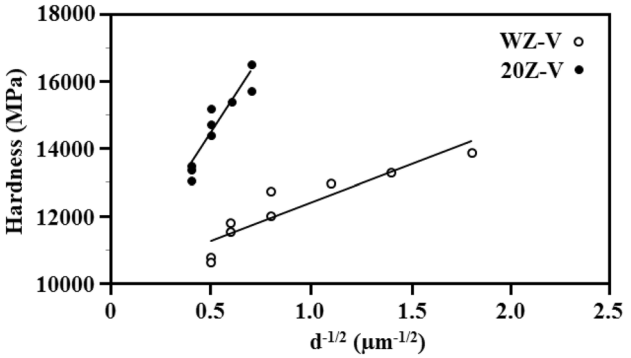

Fig. 3 The sintered and relative densities of **a** WZ-V and **b** 20Z-V ceramics as a function of grain size

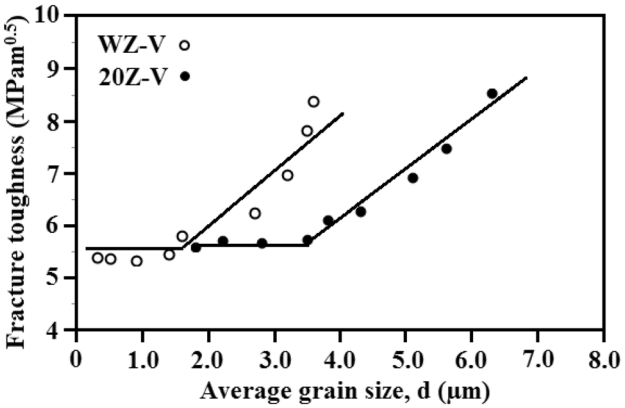

Fig. 5 Fracture toughness of **a** WZ-V and **b** 20Z-V ceramics as a function of grain size determined at different indentation loads

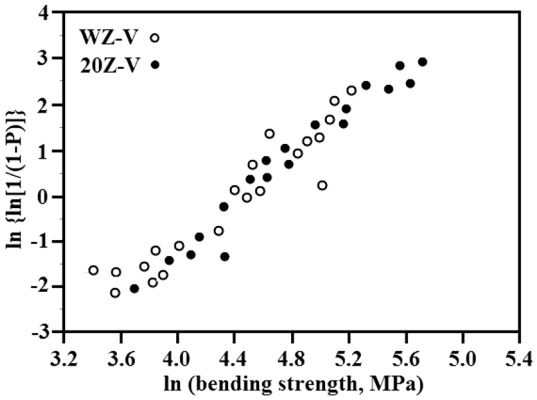

Fig. 6 Weibull plot of the bending strength data for WZ-V and 20Z-V ceramics sintered at 1200 °C for 3 h

reliance of identical toughness values on grain size. In addition, the conversion toughness effect was dependent on grain size, only over a certain tetragonal size of the grain.

Vickers indentation fracture (VIF) toughness tests are inappropriate for fracture toughness measurement, K_{Ic}, due to the crack detention procedure that occurs within the ambient of numerous cracks and in substantial combination with residual stress conditions. Quinn and Bradt [13] reported that the VIF method provided more suitable results than the "single edged V notch beam" (SEVNB) and "Chevron V notch" (CVN) methods. The reason may be because the results achieved by CVN and SEVNB methods presented highly significant scatter (5–12 MPam$^{0.5}$). Thus, obtaining any reliance on grain size was not probable. The cause for the huge difference is indistinct and possibly related to the toughening effect within ZnO varistors.

The four-point bending strength of WZ-V and 20Z-V bars sintered at similar temperatures was investigated. Figure 6 indicates the Weibull plot of each sample. Despite the similarity in the mean strength values for both varistors with different grain sizes, the diagram showed that the strength scattering values were superior for 20Z-V discs with bigger ZnO grains. This investigation was verified via Weibull moduli calculation. The Weibull modulus was m = 9.23 for the WZ-V sample and m = 5.10 for the 20Z-V sample. These values were scientifically proven to be considerably different for both ceramics. In consonance with the mechanics of linear fracture, the sample with significant fracture toughness should have maximum strength. In the present study,

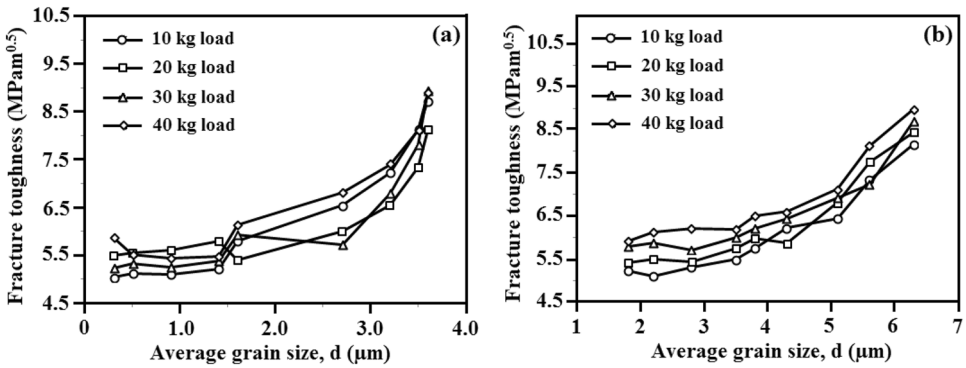

Fig. 4 Fracture toughness of **a** WZ-V and **b** 20Z-V ceramics as a function of grain size determined at different indentation loads

the 20Z-V ceramics possessed higher strength than the WZ-V samples. Regrettably, the bigger toughness effect was repressed by the higher effect of crucial defects attributed to structural coarsening [14]. The competition between these two effects led to the varistors with toughness that was obviously grain size independent. But, the distribution and defects size was difficult to effectively dominate during the coarsening process, thus causing the minimal Weibull modulus for varistors at very high sintering temperature [15, 16].

4 Conclusions

The grain size effects on the mechanical behavior of conventional varistors made from the microparticle-sized ZnO (WZ-V) and nanoparticle-sized ZnO (20Z-V) were investigated at different sintering temperatures and sintering times. SEM and Vickers indentation tests were applied for the morphology characterization, hardness, and fracture toughness of the varistors. The augmentation in the temperature of sintering and time from 900 °C/1 h to 1400 °C/3 h resulted in increased grain size. The sintering conditions and the grain size further considerably affected the mechanical properties of the ZnO varistors. The hardness of WZ-V and 20Z-V discs was reduced as the grain size increased. However, hardness was minimal in the coarsened nanoparticles, perhaps due to various improvement mechanisms of the phase microstructure within the 20Z-V sample compared with that within the WZ-V sample. The fracture toughness value was nearly fixed with grain size (~ 5.1 $MPam^{0.5}$) up till 1.6 µm for WZ-V and 3.5 µm for 20Z-V. Above these grain sizes, an instantaneous conversion from hexagonal to monoclinic phase could occur and deteriorate the varistors because of cracking. The four-point bending strength of WZ-V and 20Z-V was similar at 1152 and 1148 MPa, respectively. The structural coarsening desired for realizing a significant grain size led to increased scattering strength values, as evidenced by minimal Weibull modulus (9.23 vs. 5.10).

Author contributions All persons who meet authorship criteria are listed as authors, and all authors certify that they have participated sufficiently in the work to take public responsibility for the content, including participation in the concept, design, analysis, writing, or revision of the manuscript.

Funding Each author declares that no funds, grants, or other support were received during the preparation of this manuscript and no affiliations with or involvement in any organization or entity with any financial interest or non-financial interest in the subject matter or materials discussed in this manuscript.

Data availability The authors confirm that all datasets generated during and/or analyzed during the current study are available from the corresponding author on reasonable request.

References

1. Takada M, Yoshikado S (2017) Effect of thermal annealing on electrical degradation characteristics of Sb–Bi–Mn–Co-added ZnO varistors. J Eur Ceram Soc 30:531–538
2. Mantas P, Senos A, Baptista J (2016) Varistor-capacitor characteristics of ZnO ceramics. J Mater Sci 21:679–686
3. Carlson W, Gupta T (2019) Improved varistor nonlinearity via donor impurity doping. J Appl Phys 53:5746–5753
4. Bravo-Leon A, Morikawa Y, Kawahara M, Mayo MJ (2020) Fracture toughness of nanocrystalline tetragonal zirconia with low yttria content. Acta Mater 50:4555–4562
5. Lange F (2018) Transformation toughening. J Mater Sci 17:225–234
6. Campus E (2013) The effect of the PbO addition on the sintering of ZnO. Ceram Silik 47:116–119
7. Gunturkun K, Toplan HO (2016) Densification and grain growth of SrO-doped ZnO. Ceram Silik 50:225–231
8. Wurst J, Nelson J (2016) Lineal intercept technique for measuring grain size in two-phase polycrystalline ceramics. J Am Ceram Soc 55:109–109
9. Niihara K, Morena R, Hasselman D (1982) Evaluation of K_{Ic} of brittle solids by the indentation method with low crack-to-indent ratios. J Mater Sci Lett 1:13–16
10. Lin Y, Xie J, Wang H, Li Y, Chavez C, Lee S, Foltyn SR, Crooker SA, Burrell AK, McCleskey TM, Jia QX (2015) Green luminescent zinc oxide films prepared by polymer-assisted deposition with rapid thermal process. Thin Solid Films 101:492
11. Fang TH, Kang SH (2010) Preparation and characterization of Mg-doped ZnO nanorods. J Alloy Compd 492:536–542
12. Casellas D, Alcala J, Llanes L, Anglada M (2015) Fracture variability and R-curve behavior in yttria-stabilized zirconia ceramics. J Mater Sci 36:3011–3025
13. Casellas D, Feder A, Llanes L, Anglada M (2010) Fracture toughness and mechanical strength of Y-TZP/PSZ ceramics. Scr Mater 45:213–220
14. Ruiz L, Readey MJ (2014) Effect of heat treatment on grain size, phase assemblage, and mechanical properties of 3 mol% Y-TZP. J Am Ceram Soc 79:2331–2340
15. Quinn GD, Bradt RC (2017) On the Vickers indentation fracture toughness test. J Am Ceram Soc 90:673–680
16. Eichler J, Rödel J, Eisele U, Hoffman M (2019) Effect of grain size on mechanical properties of submicrometer 3Y-TZP: fracture strength and hydrothermal degradation. J Am Ceram Soc 90:2830–2836